Reconstructing the structure of directed and weighted networks of nonlinear oscillators

Francesco Alderisio, Gianfranco Fiore, and Mario di Bernardo*
Department of Engineering Mathematics, Merchant Venturers Building, University of Bristol, Woodland Road, Clifton, Bristol BS8 1UB, United Kingdom
(Received 2 December 2016; published 5 April 2017)

The formalism of complex networks is extensively employed to describe the dynamics of interacting agents in several applications. The features of the connections among the nodes in a network are not always provided beforehand, hence the problem of appropriately inferring them often arises. Here, we present a method to reconstruct directed and weighted topologies of networks of heterogeneous nonlinear oscillators. We illustrate the theory on a set of representative examples.

DOI: 10.1103/PhysRevE.95.042302

I. INTRODUCTION

The study of complex networks provides a rigorous formalism [1–4] to describe phenomena involving populations of interacting agents in fields as diverse as physics, engineering, biology, chemistry, social science, and the Internet [5–8].

Often in applications, the topology of the interactions (links) among the agents (nodes) in a network is not known *a priori*. In these cases the structure of the network must be reconstructed from measurements of the nodes' dynamics; a problem often known in the literature as *network reconstruction* or *network inference*. The need for network inference strategies arises in several contexts, e.g., reconstructing functional activation or repression links in gene regulatory networks [9–11] or causal relationships in stochastic processes [12], understanding the structure of social interactions in a group from communication data [13–15], and inferring functional relationships between areas in the brain from electroencephalogram (EEG) data [16] or in physiological systems [17].

A notable case of interest is that of reconstructing the structure of networks whose nodes exhibit oscillatory dynamics (e.g., neurons, cellular cycles, synthetic biological oscillators, groups of walking autonomous robots). For these networks, several reconstruction approaches have been proposed. Examples include the methodology presented in [18], dealing with the problem of inferring directed and weighted topologies of networks of Hindmarsh-Rose neurons and Lorenz oscillators; the strategy discussed in [19], investigating community detection in undirected and unweighted networks of Kuramoto oscillators [20]; the techniques developed in [21], addressing the issue of reconstructing directed topologies of small networks of coupled phase oscillators; and the methodology presented in [22], dealing with the reconstruction of directed weighted networks of coupled phase oscillators driven by temporarily constant input signals. Recent approaches to inferring the structural connectivity of a network from its dynamics have also been reviewed in [23].

Previous methods suffer from several drawbacks. Often they can only reconstruct undirected networks and do not include an *ex post* analysis of the reconstructed topology to isolate the presence of false positives (reconstructed links that do not exist in the real network), or if they do, no systematic method is presented on how to select cutoff thresholds to remove them [19]. The only exceptions are the works presented in [11,24]. However, such methodologies require the observed dependency matrix to be either invertible or diagonalizable, and have order $O(n^3)$ of computational complexity (with n being the number of nodes in the network), as opposed to our algorithm which does not make any assumption on the structure of the inferred interactions and has lower computational complexity (as discussed later in the text).

The aim of this work is to present REDRAW (reconstruction of directed and weighted topologies), a method for inferring directed and weighted topologies of networks of nonlinear oscillators. REDRAW radically extends the strategy in [19], which was originally conceived to only detect communities in undirected and unweighted networks of Kuramoto oscillators [25,26]. In what follows, we first describe the approach including a systematic algorithm to perform the *ex post* analysis of the reconstructed network and select appropriate cutoff thresholds to remove false positives. We then validate the method on a number of representative examples, including a set of real-world networks obtained from [27–31], highlighting its advantages and limitations.

II. MATERIALS AND METHODS

We start by considering a network of n nonlinearly coupled heterogeneous oscillators described by

$$\dot{x}_i = f_i(x_i) + \frac{c}{n}\sum_{j=1}^{n} a_{ij} g(x_i, x_j),\ i = 1,2,\ldots,n, \qquad (1)$$

where $x_i \in \mathbb{R}^p$ is the p-dimensional state of the ith oscillator, f_i denotes its dynamics, g is a generic nonlinear coupling function, $c > 0$ represents the global coupling strength among all nodes in the network, and a_{ij} represents the local influence that node j has on node i. For directed and weighted topologies, in general $a_{ij} \neq a_{ji}$ with $a_{ij} \geqslant 0\ \forall i,j$. By means of standard techniques [20], the system in Eq. (1) can be reduced

*Also at the Department of Electrical Engineering and Information Technology, University of Naples Federico II, Via Claudio 21, 80125 Naples, Italy; m.dibernardo@bristol.ac.uk

to a network of nonlinear phase-coupled oscillators:

$$\dot{\theta}_i = \omega_i + \frac{c}{n}\sum_{j=1}^{n} a_{ij}\Gamma(\theta_j - \theta_i),\ i = 1,2,\ldots,n, \qquad (2)$$

where $\theta_i \in [-\pi,\pi]$ represents the phase of the ith oscillator, $\omega_i > 0$ is its natural frequency, and $\Gamma(\theta_j - \theta_i)$ is a generic 2π-periodic function.

We assume that a dataset of $K \times n$ time series of length T is available. This is obtained by acquiring n time series of duration $T > 0$ (one for each of the n oscillators in the network of interest) during K experiments (or simulations) where nodes are started from different initial conditions and *phase locking* is achieved (see Sec. 1 of the Supplemental Material for the definition of "phase locking" [32]).

The goal of REDRAW is to reconstruct the topology of the network by inferring, from the data, the presence and directions of links between the oscillators. The method also captures the relative strength of the interactions among nodes by establishing which links are stronger than others. However, it does not aim at estimating the precise value of the edge weights. Note that no perfect knowledge of the system's dynamics is necessary for our method. The only assumption is that the measured phase differences among the oscillators give an indication of the strength and direction of their mutual influence.

REDRAW is based on the following six steps.

Step 1. The relative phase $\Delta\theta_{ij,k}(t) = \theta_{i,k}(t) - \theta_{j,k}(t) \in [-\pi,\pi]$, $\forall k = 1,\ldots,K$ with $t \in [0,T]$ is evaluated for every pair of nodes in each of the K experiments. Negative values of $\Delta\theta_{ij,k}(t)$ indicate that node i lags behind node j at time instant t of the kth experiment.

Step 2. The parameter $\zeta_{ij,k}(t)$, representing the influence of node j on node i at time t of the kth experiment, is defined as

$$\zeta_{ij,k}(t) := \begin{cases} \frac{1+h[\Delta\theta_{ij,k}(t)]}{2}, & \Delta\theta_{ij,k}(t) \leqslant 0 \\ 0, & \Delta\theta_{ij,k}(t) > 0 \end{cases} \qquad (3)$$

and is calculated from the available data for all pairs of nodes in the network, where h is an even function in the interval $[-\pi,\pi]$ characterized by the following properties: (i) it takes its maximum value 1 in the origin [e.g., $h(0) = 1$]; (ii) it takes its minimum values -1 at the extremes of its domain [e.g., $h(-\pi) = h(\pi) = -1$]; (iii) it is monotonically increasing in the left-half interval $[-\pi,0]$ and monotonically decreasing in the right-half interval $[0,\pi]$. Note that $\zeta_{ij,k}(t) \neq \zeta_{ji,k}(t)$ and that $\zeta_{ij,k}(t) \in [0,1]$, where $\zeta_{ij,k}(t) = 1$ represents the maximum level of influence that node j has on node i. When $\Delta\theta_{ij,k}(t) > 0$, agent j lags behind agent i, hence the influence that the former has on the latter is set to 0.

Step 3. The time average of the influence parameter defined in Eq. (3) is evaluated for each pair of nodes as

$$\rho_{ij,k} := \frac{1}{T}\int_0^T \zeta_{ij,k}(t)\,dt. \qquad (4)$$

Step 4. The weight of the link directed from node j to node i is computed for every pair of nodes by averaging the quantity defined in Eq. (4) over the total number of experiments as

$$\rho_{ij} := \frac{1}{K}\sum_{k=1}^{K} \rho_{ij,k}. \qquad (5)$$

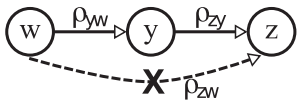

FIG. 1. Illustration of the modified data processing inequality described in Step 5. Parameter ρ_{zw} is set to 0 as long as the three following conditions are verified simultaneously: (1) $\rho_{zw} < \rho_{yw}$, (2) $\rho_{zw} < \rho_{zy}$, (3) $\rho_{zw} < \nu$, where ν is a threshold value.

Step 5. Links whose ρ_{ij} is null are discarded from the reconstructed network. Non-zero weights ρ_{ij} are checked among all triplets of connected nodes so that, on the basis of their intensity, one can be possibly regarded as a false connection and set to zero (the corresponding link is then removed). As an example, consider a triplet of three connected nodes, say w, y, and z (Fig. 1). If the weight ρ_{zw} between w and z is lower than a certain threshold $0 \leqslant \nu < 1$ and is also lower than both the weight ρ_{yw} between w and y and the weight ρ_{zy} between y and z, then ρ_{zw} is set to 0 and the link between the pair (w,z) is removed as it can be regarded as an indirect effect of w on z through node y. This is a modified version of the standard data processing inequality (DPI) often used in network reconstruction methods [33]. Note that the higher the value of ν, the fewer connected triplets are found in the network.

Step 6. Network thresholding: all parameters ρ_{ij} whose value is below a certain threshold μ are set to 0, with $0 \leqslant \mu \leqslant \nu$ (the higher the value of μ, the sparser is the reconstructed network structure).

Four standard metrics are used to assess the performance of REDRAW [34]. They are the positive predicted value (PPV), the accuracy rate (ACC), the true positive rate (TPR), and the false positive rate (FPR). Denoting with N_{TP}, N_{FP}, N_{TN}, N_{FN}, and $N_{TOT} := n(n-1)$ the total number of true positives, false positives, true negatives, false negatives, and possible links among all the nodes in the network, respectively, such metrics are defined as

$$\mathrm{PPV} := \frac{N_{TP}}{N_{TP}+N_{FP}}, \quad \mathrm{ACC} := \frac{N_{TP}+N_{TN}}{N_{TOT}},$$

$$\mathrm{TPR} := \frac{N_{TP}}{N_{TP}+N_{FN}}, \quad \mathrm{FPR} := \frac{N_{FP}}{N_{FP}+N_{TN}}.$$

Since the interactions between $n(n-1)$ pairs of nodes have to be inferred for each available experiment, REDRAW has order $O(Kn^2)$ of computational complexity. On the other hand, since the performance metrics are independent of the number of numerical experiments available, their application has order $O(n^2)$.

Remark 1. If phase locking is not achieved by the oscillators in the network, either no links or few weak links are inferred according to Eq. (5). Therefore, the influence that the phase of each node has on that of the others is negligible, hence the strength of the interactions among the oscillators is not sufficiently high for them to form any clusters.

Remark 2. The time interval $[0,T]$ can be partitioned in L time windows $[t_l,t_{l+1}]$ of length ΔT_l, with $l = 0,\ldots,L-1$ so that the network topology can be reconstructed over each subinterval to show how the nodes' interactions evolve

over time. The choice of ΔT_l is dependent on the specific application of interest (e.g., nodes' temporal dynamics).

III. RESULTS

To validate and illustrate REDRAW we consider a network of n nonuniform Kuramoto oscillators [35,36], employed as a model generating the data to test the algorithm. It is obtained by setting $\Gamma(\theta_j - \theta_i) = \sin(\theta_j - \theta_i - \phi_{ij})$ as an instance of Eq. (2), described by

$$\dot{\theta}_i = \omega_i + \frac{c}{n}\sum_{j=1}^{n} a_{ij}\sin(\theta_j - \theta_i - \phi_{ij}), \quad i=1,2,\ldots,n. \tag{6}$$

The phase shift

$$\phi_{ij} := \begin{cases} \frac{\phi}{a_{ij}}, & a_{ij} > 0 \\ 0, & a_{ij} = 0 \end{cases} \tag{7}$$

represents how much node i lags behind node j, with $\phi_{ij} \in [0, \frac{\pi}{2}]$. Note that the higher the influence a_{ij} that node j has on node i, the lower the phase shift ϕ_{ij} (i.e., the less node i lags behind node j). Furthermore, we choose $h(\theta) = \cos(\theta)$ in Eq. (3).

In contrast to previous methods, we provide guidelines on the selection of the thresholds ν and μ in Steps 5 and 6, by performing a systematic analysis of how the performance metrics change as the thresholds are varied when inferring *in silico* known ensembles (in general different from the original system to be reconstructed) of nonlinear oscillator networks (see Sec. 2 of the Supplemental Material for details on the algorithm employed to select thresholds ν and μ [32]). Specifically, we applied the algorithm to reconstruct N randomly generated graphs following the Erdös-Rényi model [37,38] as well as networks generated using the Barabási-Albert method [39], for ensembles of nonuniform Kuramoto oscillators of different size n. Note that any topology and oscillatory dynamics could be employed, however for the latter it is sensible to choose the same model as that of the system it is desired to reconstruct when information is given on the dynamics of its nodes. For both models, we evaluated what average values of ν and μ lead to acceptable reconstruction metrics, and propose that these values should then be selected when inferring an unknown topology (Fig. 2).

Remark 3. If the uncoupled dynamics is much larger than the coupling [e.g., $\omega_i \gg \frac{c}{n}$ in Eq. (6)], some oscillators may not be phase locked with their neighbors even though they share a connection. Therefore, in the following numerical examples we assume that the natural frequencies of the oscillators are all bounded.

We start by applying our method to reconstruct the four different topologies in Figs. 3(a)–3(d). Specifically, the values of the natural frequencies ω_i were randomly drawn from the standard uniform distribution on the interval [1,2] rad s^{-1}, and so were the initial conditions $\theta_i(0)$ from the interval $[-\pi,\pi]$, $i = 1,\ldots,4$. The model parameters were set to $c = 10$ and $\phi = \frac{\pi}{4}$ so that phase locking could be achieved. For each topology, a synthetic dataset of $K = 50$ experiments of duration $T = 30$ s was obtained assuming the structure of the network to be unknown. Thresholds were set to $\nu = 0.9$ and $\mu = 0.7$ from Figs. 2(a) and 2(c).

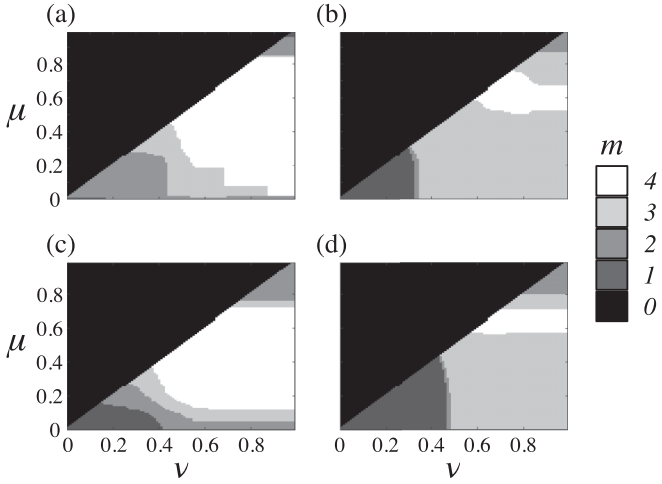

FIG. 2. Selection of thresholds for networks of n nonuniform Kuramoto oscillators. Acceptable ranges within which ν (x axis) and μ (y axis) should take values when reconstructing an unknown network of $n = 4$ (a),(c) or $n = 20$ (b),(d) oscillators are depicted as shades-of-grey maps; m denotes the number of metrics for which acceptable values are achieved when *in silico* reconstructing known test topologies. Specifically, (a) and (b) refer to the metrics obtained when employing random graphs following the Erdös-Rényi model as test topologies, whereas (c) and (d) refer to those obtained for networks generated using the Barabási-Albert method. The parameters of the oscillators were set so as to achieve phase locking. The lighter the color of the area where (ν,μ) belongs, the higher m, hence the more sensible the choice of the thresholds. Ideally, the thresholds to be used when inferring unknown topologies should be selected within white regions where ν and μ lead to acceptable values for all the four metrics here employed. See Sec. 2 of the Supplemental Material [32] for more details.

The reconstructed networks are represented in Figs. 3(e)–3(h), respectively. For each topology, neither missing links nor false positives are found, and the directionality of the links is correctly inferred for all of them (PPV = ACC = TPR = 100%, FPR = 0%). As for the weights, their magnitudes' relative relationship in the assigned topologies is correctly

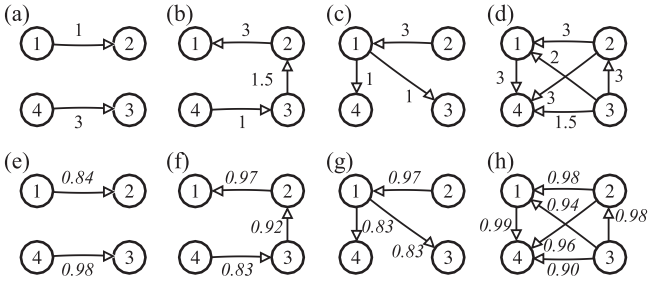

FIG. 3. Assigned and inferred topologies, $n = 4$. The topologies (a)–(d) represent those used in the numerical simulations to generate the dataset then employed to test our method. The reconstructed topologies are respectively depicted in the bottom panels (e)–(h). The numerical values on the edges of the assigned topologies represent the values of a_{ij} in the model described in Eq. (6), whereas the italic numerical values on the edges of the inferred topologies represent parameters ρ_{ij} estimated by REDRAW.

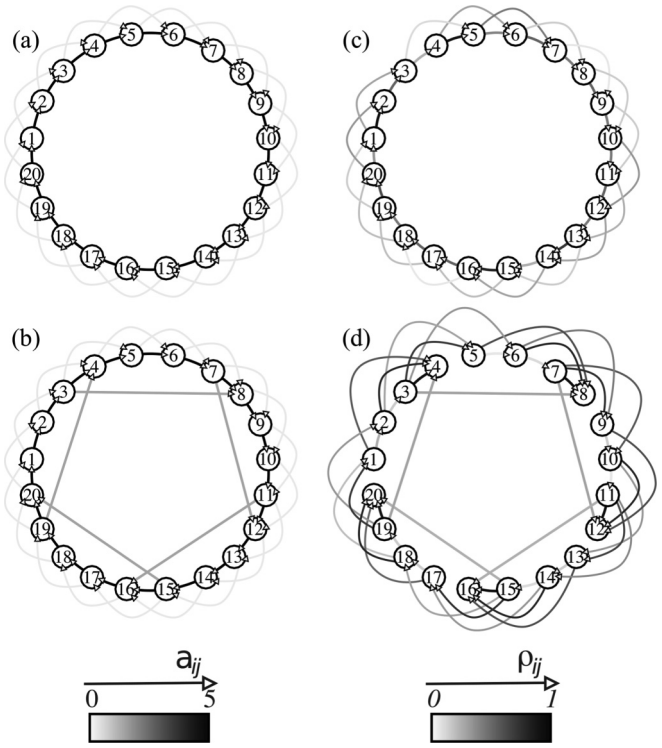

FIG. 4. Assigned and inferred topologies, $n = 20$. The regular network (a) and that obtained by some long-distance rewiring (b) on the left-hand side represent the topologies used in the numerical simulations to generate the dataset then employed to test our method. The reconstructed topologies are respectively depicted on the right-hand side (c),(d). Different scales of gray quantify the numerical value of a_{ij} for the assigned topologies, and ρ_{ij} estimated by REDRAW for the inferred ones.

inferred as well. For instance, note how $a_{34} < a_{23} < a_{12}$ in Fig. 3(b) corresponds to $\rho_{34} < \rho_{23} < \rho_{12}$ in Fig. 3(f), or how $a_{31} = a_{41} < a_{12}$ in Fig. 3(c) corresponds to $\rho_{31} = \rho_{41} < \rho_{12}$ in Fig. 3(g).

The evolution over time of the reconstructed network with topology represented in Fig. 3(c) was inferred over time windows of length $\Delta T_l = \Delta T = 0.5$s, and is shown in Sec. 4 of the Supplemental Material [32]. Analogous results are found for the other topologies (data not shown).

Next, we tested REDRAW on larger, more challenging networks of $n = 17$ nodes. The structures being considered were obtained by interconnecting four subnetworks with the structure represented in Fig. 3(d), either through a central hub in a *geometric graph* configuration [40], or as the *Ravasz-Barabási graph* [3]. Details on the results obtained for the reconstruction of such topologies can be found in Sec. 4 of the Supplemental Material [32].

As a further validation of the methodology, we used REDRAW to reconstruct the networks of $n = 20$ nodes shown in Fig. 4, both assumed to be unknown. The coupling strength among nodes was set as $c = 50$, and the thresholds of the algorithm to $\nu = 0.65$ and $\mu = 0.60$ from Figs. 2(b) and 2(d). All the other parameters were selected as before.

We find that the directionality and weights of all edges in the regular network [Fig. 4(a)] are correctly inferred [Fig. 4(c)], with the only exception of a missing link from node 2 to node 4.

The introduction of five long-distance edges [Fig. 4(b)] is well captured by the topology inferred in Fig. 4(d), leading to the formation of an equal number of clusters [nodes 1–4, 5–8, 9–12, 13–16, and 17–20]. For each of the five nodes being influenced by one of the additional links (nodes 4, 8, 12, 16, 20), no outgoing links are inferred. This is a result of the model described in Eq. (6): for instance, the phase of node 4 is lowered by the influence of node 19, thus leading to higher mismatches of the former with nodes 5 and 6 (similar reasoning can be carried out for nodes 8, 12, 16, and 20). However, note that such edges can be inferred when selecting lower values for the thresholds.

Lastly, we applied REDRAW to reconstruct some real-world network topologies from the literature [27–31], and explored the effects of noise and uncertainty on the measured phases (see Sec. 5 of the Supplemental Material for the effects of noise and uncertainty on the measured phases [32]).

The values of the four reconstruction metrics are detailed in Table I for the various topologies considered in this work, together with their structural parameters, the value of the coupling strength c used in Eq. (6) and selected in order for the network to achieve phase locking, and that of the thresholds ν and μ used for the reconstruction and selected according to Sec. 2 of the Supplemental Material [32]. All other parameters were kept as in the previous examples. Assuming PPV, ACC, TPR $> 50\%$ for the first three metrics and FPR $< 10\%$ for the last one as acceptability criteria, Table I shows the effectiveness of REDRAW in inferring networks of different size (the criteria are met in 91% of the cases).

For all the topologies considered in this work, we quantified the performance metrics for different numbers of experiments K and observed how, for a sufficiently high number of repetitions, REDRAW is not sensitive to the specific value of K. For the sake of brevity, we reported here only results for the case $K = 50$; in fact, when $K \geqslant 50$, possible fluctuations of the metrics are negligible. For more details on the performance of REDRAW for different numbers of experiments, see Sec. 3 of the Supplemental Material [32].

Remark 4. Suppose an external field drives a set of physically disconnected nodes towards the same trajectory. If only the signals generated by such nodes were provided and no information was given on the presence of the forcing field, false positives would be inferred by REDRAW. However, if the signal generated by the forcing field was available as well, the external source could be treated as an additional node in the network and the performance of the algorithm would significantly improve by means of the DPI techniques of Step 5.

IV. CONCLUSION AND DISCUSSION

We presented an effective reconstruction method to infer directed and weighted topologies of networks of heterogeneous nonlinear oscillators from data on their dynamics. We tested the strategy on a number of different examples, showing that in all cases the methodology guarantees good accuracy and an extremely low number of false positives, which

TABLE I. Validation of REDRAW. This table shows the four performance metrics obtained for different topologies, together with their own number of nodes n and edges e, respectively. The values of coupling strength c and thresholds ν and μ employed in the numerical simulations are detailed as well.

Topologies	**n**	**e**	**c**	ν	μ	PPV (%)	ACC (%)	TPR (%)	FPR (%)
Enzyme-catalyzed reaction pathway [27]	8	7	20	0.90	0.75	100	100	100	0
Songbird brain [28]	12	13	35	0.90	0.65	63	93	77	5
Bank stocks connections [29]	16	32	40	0.80	0.70	56	87	16	2
Regular network	20	40	50	0.65	0.60	100	99	97	0
Rewired network	20	45	50	0.65	0.60	67	92	67	4
Human PPI [30]	23	22	40	0.80	0.50	100	98	45	0
Human PPI [30]	25	27	50	0.80	0.65	56	96	44	2
Hainan Power Grid Company [31]	48	63	150	0.60	0.60	52	97	62	2

might occur when physically disconnected nodes are coincidentally characterized by similar oscillation frequencies and phases.

REDRAW can be applied to reconstruct the interactions among any nodes exhibiting oscillatory dynamics, as long as their phase trajectories are available. In this work, we tested the algorithm on networks of Kuramoto oscillators only as a case study. Other possibilities include, for instance, networks of Lorentz or Rössler oscillators, whose phases can be estimated by means of the techniques proposed in [41,42].

Currently, we are applying the algorithm to reconstruct networks of social interactions in groups of individuals moving in synchrony [43–45]. Such results are beyond the scope of this work and will be presented elsewhere.

ACKNOWLEDGMENTS

The authors wish to acknowledge support from the European Project AlterEgo FP7-ICT-2011-9, Topic ICT-2011.2.1 - Cognitive Systems and Robotics, Grant No. 600610.

[1] S. H. Strogatz, Nature (London) **410**, 268 (2001).
[2] R. Albert and A.-L. Barabási, Rev. Mod. Phys. **74**, 47 (2002).
[3] E. Ravasz and A.-L. Barabási, Phys. Rev. E **67**, 026112 (2003).
[4] S. Boccaletti, V. Latora, Y. Moreno, M. Chavez, and D.-U. Hwang, Phys. Rep. **424**, 175 (2006).
[5] M. Buchanan, *Nexus: Small Worlds and the Groundbreaking Theory of Networks* (Norton, New York, 2003).
[6] A.-L. Barabasi and Z. N. Oltvai, Nat. Rev. Gen. **5**, 101 (2004).
[7] A. Arenas, A. Díaz-Guilera, J. Kurths, Y. Moreno, and C. Zhou, Phys. Rep. **469**, 93 (2008).
[8] A. Cardillo, G. Petri, V. Nicosia, R. Sinatra, J. Gómez-Gardeñes, and V. Latora, Phys. Rev. E **90**, 052825 (2014).
[9] E. Crampin, S. Schnell, and P. McSharry, Prog. Biophys. Mol. Biol. **86**, 77 (2004).
[10] M. Bansal, V. Belcastro, A. Ambesi-Impiombato, and D. di Bernardo, Mol. Syst. Biol. **3**, 78 (2007).
[11] B. Barzel and A.-L. Barabási, Nat. Biotechnol. **31**, 720 (2013).
[12] J. Sun, D. Taylor, and E. M. Bollt, SIAM J. Appl. Dyn. Syst. **14**, 73 (2015).
[13] J. P. Bagrow and E. M. Bollt, Phys. Rev. E **72**, 046108 (2005).
[14] J. Sun and E. M. Bollt, Phys. D (Amsterdam, Neth.) **267**, 49 (2014).
[15] A. F. Villaverde and J. R. Banga, J. R. Soc. Interface **11**, 20130505 (2014).
[16] M. Staniek and K. Lehnertz, Phys. Rev. Lett. **100**, 158101 (2008).
[17] T. Schreiber, Phys. Rev. Lett. **85**, 461 (2000).
[18] D. Yu, M. Righero, and L. Kocarev, Phys. Rev. Lett. **97**, 188701 (2006).
[19] A. Arenas, A. Díaz-Guilera, and C. J. Pérez-Vicente, Phys. Rev. Lett. **96**, 114102 (2006).
[20] Y. Kuramoto, *Chemical Oscillations, Waves, and Turbulence* (Springer Science & Business Media, New York, 2012), Vol. 19.
[21] B. Kralemann, A. Pikovsky, and M. Rosenblum, Chaos **21**, 025104 (2011).
[22] M. Timme, Phys. Rev. Lett. **98**, 224101 (2007).
[23] M. Timme and J. Casadiego, J. Phys. A: Math. Theor. **47**, 343001 (2014).
[24] S. Feizi, D. Marbach, M. Médard, and M. Kellis, Nat. Biotechnol. **31**, 726 (2013).
[25] J. A. Acebrón, L. L. Bonilla, C. J. P. Vicente, F. Ritort, and R. Spigler, Rev. Mod. Phys. **77**, 137 (2005).
[26] A. Antonioni and A. Cardillo, arXiv:1607.03186.
[27] A. F. Villaverde, J. Ross, F. Morán, and J. R. Banga, PLoS One **9**, e96732 (2014).
[28] K. Basso, A. A. Margolin, G. Stolovitzky, U. Klein, R. Dalla-Favera, and A. Califano, Nat. Genet. **37**, 382 (2005).
[29] F. X. Diebold and K. Yılmaz, J. Econometrics **182**, 119 (2014).
[30] A. Vinayagam, U. Stelzl, R. Foulle, S. Plassmann, M. Zenkner, J. Timm, H. E. Assmus, M. A. Andrade-Navarro, and E. E. Wanker, Sci. Signal. **4**, rs8 (2011).
[31] L. Chang and Z. Wu, Int. J. Elec. Power & Energy Syst. **33**, 1410 (2011).
[32] See Supplemental Material at http://link.aps.org/supplemental/10.1103/PhysRevE.95.042302 for definition of phase-locking, details on the algorithm employed to select thresholds μ and ν, reconstruction of further networks, and results obtained when considering different number of available experiments, noise, and uncertainty on the measured phases.
[33] A. A. Margolin, I. Nemenman, K. Basso, C. Wiggins, G. Stolovitzky, R. D. Favera, and A. Califano, BMC Bioinf. **7**, S7 (2006).

[34] B. DasGupta and J. Liang, *Models and Algorithms for Biomolecules and Molecular Networks* (John Wiley & Sons, New York, 2016).
[35] F. Dörfler and F. Bullo, SIAM J. Control Optim. **50**, 1616 (2012).
[36] W.-Y. Zhang, C. Yang, Z.-H. Guan, Z.-W. Liu, M. Chi, and G.-L. Zheng, Neurocomputing **218**, 216 (2016).
[37] P. Erdös and A. Rényi, Publ. Math. Debrecen **6**, 290 (1959).
[38] P. Erdös and A. Rényi, Publ. Math. Inst. Hungar. Acad. Sci. **5**, 17 (1960).
[39] A.-L. Barabási and R. Albert, Science **286**, 509 (1999).
[40] J. Dall and M. Christensen, Phys. Rev. E **66**, 016121 (2002).
[41] M. Beck and K. Josić, Chaos **13**, 247 (2003).
[42] G. V. Osipov, A. S. Pikovsky, M. G. Rosenblum, and J. Kurths, Phys. Rev. E **55**, 2353 (1997).
[43] F. Alderisio, B. G. Bardy, and M. di Bernardo, Biol. Cybern. **110**, 151 (2016).
[44] F. Alderisio, G. Fiore, R. N. Salesse, B. G. Bardy, and M. di Bernardo, arXiv:1607.02175.
[45] F. Alderisio, M. Lombardi, G. Fiore, and M. di Bernardo, arXiv:1608.04652.